

Gravitational wave scattering

F. A. Handler

Bell Laboratories, West Long Branch, New Jersey
and Center for Relativity, University of Texas, Austin, Texas 78712*

Richard A. Matzner

Center for Relativity, University of Texas, Austin, Texas 78712

(Received 2 May 1980)

We consider scattering of gravitational radiation incident axially on Kerr black holes. A Jeffreys-Wentzel-Kramers-Brillouin formulation applied to a combination of the Teukolsky-Press and Chandrasekhar-Detweiler formalisms allows the integration for relatively large frequencies $|\omega|$. Many interesting structures arise in the resultant cross sections. These include glories, dips in the cross section "due to" geometrical-optics orbits near the capture orbits, preferential polarization of the scattered wave, and very strong backward scattering when the conditions for superradiance hold.

I. INTRODUCTION

The concept of a black hole, an object so condensed that even radiation cannot escape from it, was once dismissed as a prediction of relativity which was technically theoretically correct, but had no relevance to astrophysical objects. The Schwarzschild radius, i. e., the *horizon* radius, of a black hole of the mass of the sun is only 1.5 km. It seemed safe to dismiss black holes as theoretical irrelevancies.

The situation now has changed significantly. Although absolutely conclusive astronomical evidence for a black hole has not been found, very plausible candidates (e. g., Cygnus X-1) exist. Astrophysicists have had to take black holes seriously. They are part of the standard vocabulary of astrophysics, and part of the standard testing ground of astrophysical ideas.

In a similar way, theoretical investigation may turn from a concentration on the properties of a black hole to the use of black holes to test our understanding of other phenomena. A classical black hole is the gravitating object of absolutely minimal structure; it gives us the greatest likelihood of discovering the properties of the gravitational field *per se*, free of contamination of "material" modes. In more practical terms, there are many limiting situations where only the black-hole-like properties of the gravitational field are relevant, and it can be taken as the paradigmatic test body.¹

This work is concerned with the scattering of *gravitational* radiation by vacuum black holes (Schwarzschild² or Kerr³). It is an extension of work done by Matzner and Ryan.⁴ That earlier work presented catalogs of black-hole cross sections for gravitational waves with frequencies $|\omega|$ of up to $0.75/M$ (M is the mass of the black hole). For higher frequencies, phases at small l values

(l is the angular momentum value for the angular decomposition in the separation-of-variable solution) were presented. Matzner and Ryan were prevented by the cost of computer time from carrying the large- $|\omega|$ calculation to values of l large enough to be considered asymptotic. Hence they could not determine the entire summed cross section for those higher frequencies. In fact, it appears that some of their calculations for $|\omega| = 0.75/M$ which they *did* present as cross sections were not carried sufficiently far into the asymptotic regime. Neglect of large- l structure for those frequencies gave a smoothed result, certainly the conservative result one expects if fine angular structure is suppressed. Many interesting details of such structure are related to the qualitative descriptive pictures which have been developed for understanding wave scattering, and unfortunately these qualitatively enlightening features were suppressed in the Matzner-Ryan $|\omega| = 0.75/M$ summed cross sections. We display these features here (Figs. 12-14).

Section II gives the outline of a partial-wave formulation of gravitational scattering. We then discuss in Sec. III the technical improvements which allow us to carry out calculations for larger l values. The thrust of this section is toward a JWKB approximation (Rayleigh,⁵ Jeffreys,⁶ Wentzel,⁷ Kramers,⁸ Brillouin,⁹) of the radial differential equation based on Chandrasekhar and Detweiler's¹⁰ formulation of the wave-perturbation problem in the Kerr geometry.

Section IV gives results for absorption and scattered wave phases. Before introducing the full summed cross section, we recall, in Sec. V, the beautifully descriptive semiclassical theory of scattering and show the relation between the value of phases as a function of angular momentum parameter l , and the scattering cross section. It is this semiclassical theory which allows an un-

derstanding of the remarkable progression of features seen in the cross sections calculated in Sec. VI for different values of ω and for different values of the Kerr specific angular momentum a .

Section VI does not present a complete catalog of cross sections in the parameter space of ω and a . Instead we concentrate on a few particular examples which typify the behavior of the cross section, and see displayed the semiclassical wave-scattering structure of gravitational radiation scattering. Gravity waves do scatter just as electromagnetic waves do. Rainbows formed by light on spherical droplets of water have their equivalent in the scattering of gravitational radiation by black holes, even spinning black holes. The unity of the wave description of radiation should have been expected; what is remarkable is the revelation once more, in an unexpected place, of this unity.

II. GRAVITATIONAL WAVE CROSS SECTIONS

Analysis of the gravitational perturbations of the Kerr geometry (the Schwarzschild case is always treated as a limiting example) may be approached either from the Riemann-tensor approach of Teukolsky and Press,¹¹ based on the Newman-Penrose¹² (NP) formalism, or from the metric perturbation approach of Chandrasekhar and Detweiler.¹⁰ For the present authors, familiarity dictated the Teukolsky-Press form; in particular, this work is an outgrowth of that by Matzner and Ryan,⁴ who used that formulation. Connections are still required between the Riemann-tensor structure and the metric perturbations; such may be found in the literature.^{4, 10, 13} The critical element in the actual calculation of a cross section is the calculation of the radial wave function. As discussed below, we will find it expedient at a crucial point to switch from a direct calculation of the Teukolsky-Press variables to a JWKB structure based on Chandra-

sekhar and Detweiler's formalism.¹⁰ Hence, we opportunistically take the most useful from each formalism to meld into the whole.

We now review the formal analysis leading to a gravitational scattering cross section. In what follows,

$$\frac{dr^*}{dr} \equiv \frac{r^2 + a^2}{\Delta}, \quad (2.1)$$

$$\Delta = r - 2Mr + a \quad (2.2a)$$

$$= (r - r_+)(r - r_-) \quad (2.2b)$$

(defining Δ , r_+ , and r_-).

The equation satisfied by Riemann-tensor wave perturbations is separable in Boyer-Lindquist¹⁵ spheroidal coordinates. Because much of this analysis is available in the literature, we only sketch results here; symbols have their conventional meaning, and details and definitions not given here can be found in the Appendix. One has

$$\Psi_{(s)} = e^{-i\omega t} {}_s Z_l^m(\theta, \varphi; a\omega) R_{lm}(r, \omega),$$

where $\Psi_{(s)} = \Psi_0, \rho^{-4} \Psi_4$ for the spin-weight $s = +2, -2$ Riemann-tensor components, respectively. The radial equation is

$$\Delta^{-s} \frac{d}{dr} \left(\Delta^{s+1} \frac{dR}{dr} \right) + \left(\frac{K^2 - 2is(r-M)K}{\Delta} + 4ris\omega r - \lambda \right) R, \quad (2.3)$$

with

$$K = (r^2 + a^2)\omega - am,$$

and λ is related to the eigenvalue of ${}_s E_l^m$ of the angular equation (A1):

$$\lambda = {}_s E_l^m + a^2 \omega^2 - 2am\omega$$

[cf. Eq. (3.27)]. Asymptotic solutions of Eq. (2.3) take the form

$$\Psi_4^{\text{down}} \underset{r \rightarrow \infty}{\sim} \int_{-\infty}^{\infty} -\frac{d\omega'}{(\omega')^2} \frac{1}{32} \sum_{l m \bar{m}} e^{-i\omega'(r^*+t)} [(\text{Re}C + 12iM\omega'P) K_{l m \omega' P}^{\text{down}} / r^5] {}_2 Z_l^m(a\omega'), \quad (2.4)$$

$$\Psi_4^{\text{up}} \underset{r \rightarrow \infty}{\sim} \int_{-\infty}^{\infty} -\frac{d\omega'}{2} (\omega')^2 K_{l m \omega' P}^{\text{up}} (e^{i\omega'(r^*-t)}/r) {}_2 Z_l^m(a\omega') \quad (2.5)$$

with similar expressions holding for Ψ_0 . (The constant C is defined in the Appendix.) Here and subsequently, "down" refers to a mode which vanishes on g^+ (i. e., pure ingoing at infinity) while "up" refers to a mode which vanishes on g^- (pure outgoing at infinity). These forms (2.4) and (2.5) are related to asymptotic metric perturbations (in appropriate gauges; Chrzanowski *et al.*¹³) expressed in terms of the metric projected on the transverse vectors m, \bar{m} :

$$h_{m\bar{m}}^{\text{down}} \underset{r \rightarrow \infty}{\sim} \int_{-\infty}^{\infty} d\omega' \sum_{l m \bar{m}} K_{l m \omega' P}^{\text{down}} {}_2 Z_l^m(a\omega') e^{-i\omega'(r^*+t)}/r \quad (2.6)$$

and

$$h_{\bar{m}m}^{\text{up}} \underset{r \rightarrow \infty}{\sim} \int_{-\infty}^{\infty} d\omega' \sum_{l m \bar{m}} K_{l m \omega' P}^{\text{up}} {}_2 Z_l^m(a\omega') e^{i\omega'(r^*-t)}/r. \quad (2.7)$$

Since the metric perturbations are real there is a condition: $K_{l m \omega' P} = P \bar{K}_{l -m -\omega' P}$.

These formulas are relevant because the mode constants $K_{l m \omega' P}^{\text{up}}$, $K_{l m \omega' P}^{\text{down}}$ for an incident plane wave of frequency ω are easily calculated:

$$K_{l m \omega P}^{\text{down}}(\text{plane wave}) = -\frac{h\pi}{i\omega} {}_2N_{l, \tau}^2(a\omega) \times [\delta_{m2} \delta(\omega' - \omega) - P \delta_{m-2} \delta(\omega' + \omega)] \quad (2.8)$$

and

$$K_{l m \omega P}^{\text{up}}(\text{plane wave}) = -(-1)^{l+m} K_{l m \omega P}^{\text{down}}(\text{plane wave}). \quad (2.9)$$

These amplitudes are for circular polarization. If $a\omega > 0$, the waves corotate with the hole. If $a\omega < 0$, they counterrotate. Plane polarized waves are constructed by combining circular polarization amplitudes. Note also that the subscripted $K_{l m \omega P}$ is a mode constant, while the unsubscripted K of Eq. (2.3) is an explicitly defined function of r . Similarly, note the distinction between ${}_s Z_l^m$, the angular wave function, and the quantity Z which appears in Eqs. (3.17) and (A13). This latter Z is one form of the radial wave function. Unfortunately, the conventional notation for these quantities is ambiguous. We hope the context will make the meaning clear. ${}_2N_{l, \tau}^2$ is a constant related to the limiting behavior of the angular wave function ${}_s Z_l^m = e^{im\phi} {}_s S_l^m(\theta; a\omega)$ [cf. Eqs. (A11) and (A12)] and h is the wave amplitude.

We point out a curious feature of the metric perturbation approach versus the Riemann-tensor approach. In the asymptotic metric plane wave form, the two parities appear in essentially the same way. However, it is well known that the metric perturbation equations (even in the spherically symmetric case) differ for the two parities. On the other hand, the Teukolsky equation (2.3) does not depend on parity, but the asymptotic plane wave for the Riemann-tensor components does. Because the parity splitting occurs therefore explicitly in the initial data, the different parity dependence in the general solution is straightforwardly obtained. Chandrasekhar and Detweiler¹⁵ showed that the reflection and transmission coefficients (quantities obtained by taking the absolute square of the amplitudes) for the radial equation, considered as a 1-dimensional scattering problem, are the same for the two parities. It is here precisely the *phase* of the amplitudes which is important. The explicit $\text{Re}C \pm i12M\omega P$ dependence on parity leads to differences in phase shifts, which are very important in calculating the cross sections.

Equations (2.3)–(2.9) contain the fundamental equations for a scattering calculation. A solution to the radial Teukolsky equation is found (by numerical integration if necessary) with normalization adjusted so that $K^{\text{down}} = K^{\text{down}}(\text{plane wave})$, and with *scattering* boundary conditions, nothing emerging from the past horizon \mathcal{H}^- . The value of the mode coefficient K^{up} determines the scattered wave by

$$\Psi_4(\text{scatt}) \underset{r \rightarrow \infty}{\sim} \int_{-\infty}^{\infty} -\frac{d\omega'}{2} (\omega')^2 \times \sum_{l m P} \left[\tilde{K}_{l m \omega P} \frac{e^{i\omega'(r^* - t)}}{r} {}_2Z_l^m(a\omega') \right], \quad (2.10)$$

where

$$\tilde{K}_{l m \omega P} = K_{l m \omega P}^{\text{up}} - K_{l m \omega P}^{\text{down}}(\text{plane wave}). \quad (2.11)$$

Since \tilde{K} also determines the asymptotic transverse (traceless) part of the metric wave perturbation, we may directly evaluate effective energy fluxes, etc., using \tilde{K} . By using the symmetries of the angular function ${}_s S_l^m$, we obtain⁴

$$\frac{d\sigma}{d\Omega} = h^{-2} \left[\left| \sum_{l P} \tilde{k}_{l 2\omega P} {}_2S_l^2(\theta; a\omega) \right|^2 + \left| \sum_{l P} (-1)^l P \tilde{k}_{l 2\omega P} {}_2S_l^2(\pi - \theta; a\omega) \right|^2 \right], \quad (2.12)$$

while the total absorption cross section is

$$\sigma_{abs} = \sum_{l m P} h^{-2} [|k_{l m \omega P}^{\text{up}}(\text{plane wave})|^2 - |\tilde{k}_{l m \omega P}|^2] \quad (2.13)$$

(see also Unruh¹⁶).

In these two equations, \tilde{k} is defined by

$$\tilde{K}_{l m \omega' P} \equiv \tilde{k}_{l 2\omega P} \delta_{m2} \delta(\omega - \omega') + \tilde{k}_{l -2\omega P} \delta_{m-2} \delta(\omega + \omega') \quad (2.14)$$

with a similar expression linking $K^{\text{up}}(\text{plane wave})$ and $k^{\text{up}}(\text{plane wave})$.

III. MATHEMATICAL FORMULATION, PROBLEMS, RESOLUTION

Previous studies of the gravitational-wave-scattering problem used a direct numerical integration of the Teukolsky radial equation. The appearance of the term $4is\omega$ in Eq. (2.3) forces an asymptotic difference of $|2s|$ powers of r in the amplitude of the ingoing versus the outgoing solutions. A change of dependent variable, to a new variable called χ , was given by Press and Teukolsky.¹⁷ It removes this asymptotic amplitude difference but leaves the resultant second-order equation in a form in which the incoming solution is asymptotically of the form $\sim e^{2i\omega r^*}$ while the outgoing solution is asymptotically constant. The presence of this rapidly oscillating phase, together with the necessity of maintaining accuracy over a substantial number of cycles, results in impractically large integration times, even for moderate values of $|M\omega|$.⁴ The previous work was therefore

restricted to relatively small values of this parameter, and relatively small values of the angular quantum number l , since the required integration range in r is proportional to $|l/\omega|$.

When difficulties of this type arise, it is natural to consider some sort of analytical approximation that handles the rapid phase variation, and allows a more straightforward integration of the amplitude. Such an approximation is the JWKB approximation, the eikonal approximation.^{5, 6, 7, 8, 9} To proceed in this fashion we set¹⁸

$$\mathfrak{y} = (r^2 + a^2)^{1/2} \Delta^{s/2} R \quad (3.1)$$

and find (prime denotes d/dr^*)

$$\mathfrak{y}'' + \left\{ \frac{[K^2 - 2is(r-M)K + \Delta(4ir\omega s - \lambda)]}{(r^2 + a^2)^2} - G^2 - G \right\} \mathfrak{y} = 0, \quad (3.2)$$

where K is defined as in (2.3), and

$$G = s(r-M)/(r^2 + a^2) + r\Delta/(r^2 + a^2)^2. \quad (3.3)$$

Equation (3.2) is of the standard form for JWKB analysis:

$$\mathfrak{y}'' + \xi_{\mathfrak{y}} \mathfrak{y} = 0 \quad (3.4)$$

with $\xi_{\mathfrak{y}}$ asymptotically given by

$$\xi_{\mathfrak{y}} = \omega^2 + \frac{2i\omega s}{r} + O\left(\frac{1}{r^2}\right). \quad (3.5)$$

A similar asymptotic form is obtained for the χ equation. The JWKB solution is (cf. Mathews and Walker¹⁹)

$$W_{\text{JWKB}} = a_+ W_+ + a_- W_-, \quad (3.6)$$

with

$$W_{\pm} = \xi^{-1/4} \exp\left(\pm i \int \xi^{1/2} dr^*\right). \quad (3.7)$$

The constants a_{\pm} may be determined by matching the JWKB form to an exact solution W at any particular point. This gives

$$a_{\pm} = \pm \frac{1}{2} i (W W'_{\pm} - W' W_{\pm}), \quad (3.8)$$

where the right-hand side of the equation is evaluated at the match point. The W_{\pm} are not exact solutions to (3.4); we may view the deviation of the JWKB solution from the exact solution as a functional variation with match point r of the constants a_{\pm} .

For the asymptotic potential given by (3.5), the asymptotic JWKB solutions are

$$W_{\pm} \approx \xi^{-1/4} \exp[\pm i\omega(r + 2M \ln r) \mp s \ln r], \quad (3.9)$$

where the term involving M arises from the asymptotic form of dr^*/dr . The ratio of the two solutions thus varies as r^{2s} . The error accumula-

tion also obviously depends on the asymptotic behavior of ξ . We define error as the accumulated change in the ratio a_-/a_+ (integrated from the match point to any particular radius r). We find

$$(a_-/a_+)' \sim \frac{g}{\omega} r^{2s} \quad (3.10)$$

with

$$g = \frac{1}{4} \frac{\xi''}{\xi} - \frac{5}{16} \left(\frac{\xi'}{\xi}\right)^2. \quad (3.11)$$

Asymptotically, for Eq. (3.4), $g \sim r^{-2}$. [Notice that the JWKB solutions are exact solutions to $W_{\pm}'' + (\xi + g)W_{\pm} = 0$.] With this asymptotic form for g , $(a_-/a_+)' \sim r^{2(s-1)}$ and hence requires $s < \frac{1}{2}$ for convergent total error. Such an approach is thus inapplicable for the gravitational ($|s|=2$) and electromagnetic ($|s|=1$) cases, and marginally unsuitable for the neutrino case with $|s| = \frac{1}{2}$. One would have to refine the error analysis to make a definite statement about this latter case. (The formulation in terms of the variable χ , referred to above, leads to similar error estimates if cast into a JWKB form.)

We expect, however, that the JWKB inapplicability is only an artifact of the Newman-Penrose formalism, which deals *ab initio* with complexified objects. It is the imaginary term proportional to r^{-1} in Eq. (2.3) which causes the difficulty with the JWKB approximation and this type of term must have arisen from an explicit complexification of the problem. Actual metrics are, after all, real. Consider a general radial wave equation of the form

$$\frac{d^2 \phi}{dr^2} + \left(\omega^2 + \frac{2\gamma}{r} - \frac{E_l}{r^2} + V_h \right) \phi = 0, \quad (3.12)$$

where $V_h \sim O(r^{-3})$ or higher. By a suitable choice of the parameter γ and V_h and if $\phi = r\psi$, where ψ is the probability wave function, Eq. (3.12) is the quantum-mechanical Coulomb ($\gamma = Ze^2, \hbar^2/\mu = 1$) or the Newtonian gravitational ($\gamma = 2M\omega^2$) scattering problem. By letting

$$r^* = r + \frac{\gamma}{\omega^2} \ln\left(r - \frac{\gamma}{\omega^2}\right) \quad (3.13)$$

and

$$y = \left(\frac{dr^*}{dr}\right)^{1/2} \phi = r \left(\frac{dr^*}{dr}\right)^{1/2} \psi, \quad (3.14)$$

one finds that y satisfies

$$\frac{d^2 y}{dr^{*2}} + (\omega^2 - V_*) y = 0, \quad (3.15)$$

with the potential V_* asymptotically of order r^{-2} or smaller, given by

$$V_* \approx \frac{E_l - 3\gamma^2/\omega^2}{r^2} + O(r^{-3}). \quad (3.16)$$

Clearly, any scattering with a real potential which admits plane-wave solutions at infinity may be put in short-range form by a suitable choice of wave function and coordinates. If one chooses to work directly with (real) metric perturbations instead of the complex quantities of the NP formalism one then expects the Schwarzschild case should possess a choice of variable yielding the form (3.16). Indeed this is the case (cf. Ref. 15 and references therein). Since the Kerr case is asymptotically Schwarzschild, by analogy one concludes that Kerr should also possess such a form.²⁰ That this is not immediate in the analytical structure is due to the fact that the algebraic intricacy of the perturbation problem motivates the use of the complex NP formalism with a resultant potential having, in particular, complex γ [see Eq. (3.2)]. This leads naturally to a potential which is short range but in a complex variable. The resultant solutions then still differ asymptotically by several powers of r .

Since we know a suitable solution with (at least) real γ exists we seek such a form by using instead of (3.14) the most general transformation of the form $Z(r_*) = g(r)R(r) + h(r)R'$ and solve for g and h subject to the form desired of the equation for Z . Such a calculation has been performed by Chandrasekhar.¹⁰ The result is that Z satisfies

$$\left[\frac{d^2}{dr_*^2} + (\omega^2 - V_Z) \right] Z = 0, \quad (3.17)$$

where r_* is defined by

$$\frac{dr}{dr_*} = \frac{\Delta}{r^2 + a^2 - am/\omega}, \quad (3.18)$$

and where V_Z is asymptotically real, and $V_Z \sim r^{-2}$ as $r \rightarrow \infty$. The explicit dependence of Z on R and its derivative, and the explicit form of V_Z are given in the Appendix. In fact, since V_Z contains two constants determined only up to a sign, there are four physically equivalent potentials V_Z .

The detailed behavior of the potential V_Z has been discussed at length by Chandrasekhar and Detweiler in a series of papers.^{10,15,21} For our present purpose several of the general features are of importance and are distinguished by the presence or absence of superradiance. (Superradiance is the process whereby incident radiation may extract energy from the hole, increasing the amplitude of the wave.)

In the nonsuperradiant ($\omega > am/2Mr_* = \omega_s$) case, the potential is well behaved everywhere outside the horizon, differing from the usual sort of potential encountered in central potential problems only by being complex. In the superradiant case $\omega \leq \omega_s$ singularities appear outside of the horizon, and the $r(r_*)$ relation becomes double valued with

$r_* \rightarrow +\infty$ corresponding to $r \rightarrow r_+$ and $r \rightarrow \infty$.

In principle, the singularities arising in the potential present no insurmountable obstacle to numerical integration but do require special consideration at the singular points. To avoid such consideration we choose to integrate the χ equation, which is well behaved everywhere, from the horizon through the points of singularity of V_Z to a value of r at which the error in the JWKB approximation to the function Z , as given by Eq. (3.7), with W_{\pm} appropriate for Z , is small. We then match χ and its derivative to Z and its derivative and apply the JWKB approximation to the Z equation to continue the integration to large r . Because of the asymptotic form of V_Z , the JWKB analysis goes through without difficulty. Since the amplitudes of the ingoing and outgoing parts of Z are asymptotically constant, there is no difficulty in separating these parts from the asymptotic solution.

There is dramatic evidence of the advantage in using a JWKB approximation to integrate the phase directly rather than integrating the rapidly oscillating wave function itself. For instance, for $l = 7$ and $M\omega = -a/M = 0.75$ it takes more execution time (several seconds) to integrate χ directly from $r \sim 30M$ to $r \sim 40M$ than to perform the integration in (3.7) from $r \sim 30M$ to the asymptotic regime at $r \sim 400M$, a reduction of computation time by about a factor $\frac{1}{10}$. Even greater savings are realized for the larger values of l , for which integration must proceed to still larger values of r . The difference in partial absorption cross section for each l mode as calculated by the two methods is less than one part in 10^5 .

The Chandrasekhar-Detweiler equation (3.17) and the Coulomb version of (3.15) are very similar. For calculating cross sections, this similarity at once poses a problem and provides its solution. First note the similarity: the radial equation for Z in the Kerr gravitational scattering case is identical, for large l and r , to that of quantum-mechanical Coulomb scattering of spinless electrons except for the parameter choice in the $1/r^2$ term. We then have the same problem in a partial-wave calculation of the gravitational cross section as in the Coulomb problem, namely, the radial solutions only slowly approach an asymptotic form as l increases. This would force a tedious numerical integration of the radial equation for many values of l until l was large enough to transcribe the analytical asymptotic remainder and sum the cross section.

The problem is its own solution since the Coulomb case has a well-known analytical solution. Recall for a moment the usual motivation for adopting a partial-wave analysis in potential scat-

tering problems. For this one views each incoming l mode as an individual projectile of orbital angular momentum $\sim(E_l)^{1/2} \sim b\omega$, where b is an equivalent asymptotic impact parameter along the axis of incidence (see Fig. 3 and Sec. IV). For problems containing only a short-range potential V (i. e., V falls off as fast or faster than $1/r^2$ or else $V=0$ for r greater than some value r_0) those modes with $l \geq l_0 = r_0\omega$ contribute negligibly to the scattered wave; they effectively miss the potential. For such modes one may simply transcribe the asymptotic free wave solution. Hence, the radial equation need be exactly solved only for $l \leq l_0$.

In the Kerr and Coulomb cases the potential is not short range since it possesses a term in $1/r$. We then expect to have to solve the radial equation for a large range of l values to obtain a complete solution. But now the analytical Coulomb solution solves the problem for it can play the role of the asymptotic free wave in the usual partial-wave analysis. The point of using the asymptotic free wave was not that it is free but simply that it is analytically known, allowing immediate transcription for $l > l_0$. For sufficiently large l the Kerr modes, instead of missing the potential, are scattered as they would be by a pure Coulomb potential. For l less than some reasonable value we calculate the Kerr modes numerically. For the remainder of the l modes we make an appropriate identification of parameters and transcribe the analytical Coulomb result exactly.

In the Coulomb scattering problem, the wave function has the form

$$\phi_{l \text{ Coul}} \underset{r \rightarrow \infty}{\sim} -\frac{1}{2i\omega r} [(-1)^l e^{-i\omega r^*} - e^{2i\eta_l} e^{i\omega r^*}], \quad (3.19)$$

where r^* is the Coulomb radial variable defined by Eq. (3.13). It incorporates the long-range logarithmic phase in both ingoing and outgoing waves due to the $1/r$ potential. The first term on the right is the ingoing part of the mode normalized conveniently to unity. The second term on the right is the outgoing scattered piece of the wave multiplied by the phase-shift term $e^{2i\eta_l}$ incorporating the effect of the scattering by the potential. The pure Coulomb phase shift with parameters appropriate to gravitational scattering is given by

$$e^{2i\eta_l} = \frac{\Gamma(l+1-2iM\omega)}{\Gamma(l+1+2iM\omega)} \quad (3.20)$$

with Γ denoting the gamma function.²² The Kerr case is analogous to the situation when the Coulomb case is combined with a short-range nuclear

potential. The phase shifts may then be written $\delta_l = \eta_l + \Delta\delta_l$. Generally, for any given value of l , the larger ω (hence the larger the energy of the incoming wave) the larger is $\Delta\delta_l$. For a fixed ω , however, $\Delta\delta_l \rightarrow 0$ as l becomes large.

We may put the perturbation equation (3.17) for gravitational waves in the Kerr background in the form of (3.12) by letting $\phi_z = (dr/dr_*)^{1/2} Z$. Then in the large- r limit we have

$$\phi_z'' + [\omega^2 - V_z + O(r^{-4})] \left(\frac{dr_*}{dr}\right)^2 \phi_z \approx 0, \quad (3.21)$$

with the prime again denoting derivation with respect to r . Asymptotically, the potential V_z assumes the form

$$V_z \sim \frac{E_l + a^2\omega^2 - 2a\omega m}{r^2} + O(r^{-3}). \quad (3.22)$$

Now we may expand dr_*/dr to obtain the large- r limit of Eq. (3.21) [cf. (3.15) and (3.16)]:

$$\phi_z'' + \left(\omega^2 + \frac{4M\omega^2}{r} + \frac{12M^2\omega^2 - E_l - a^2\omega^2 + 2a\omega m}{r^2}\right) \phi_z \approx 0. \quad (3.23)$$

This is essentially an approximation in $l/\omega \gg 1$ since for fixed ω the classical turning point increases approximately as l .

First consider the Schwarzschild case $a=0$. In this case the angular eigenvalues are $E_l = l(l+1)$. Now Eq. (3.23) is identical to the usual Coulomb radial equation, except for the appearance of the term $12M^2\omega^2$ in Eq. (3.23). If we then define

$$\tilde{l} = -\frac{1}{2} + \frac{1}{2}[1 - 48M^2\omega^2 + 4l(l+1)]^{1/2}, \quad (3.24)$$

Eq. (3.23) is identical to a Coulomb problem with $l(l+1)$ replaced by $\tilde{l}(\tilde{l}+1)$. For large l , $l > L$ say, the Schwarzschild phase shifts are thus independent of parity since both parities approach the Coulomb form [cf. Eq. (4.12)] and are given by Eq. (3.20) with l replaced by \tilde{l} . Typically L is a function of ω .

In the Schwarzschild case we can then use, as a good approximation to the cross section,

$$\frac{d\sigma}{d\Omega} \approx \frac{1}{h^2} \left[\left| \sum_P \left(\sum_{l=2}^L \tilde{k}_{l2\omega P} + \sum_{l=L+1}^{\infty} \tilde{k}_{l2\omega P}^{\text{Coul}} \right) {}_{-2}S_l^2(\theta; 0) \right|^2 + \left| \sum_P \sum_{l=2}^L (-1)^l P \tilde{k}_{l2\omega P} {}_{-2}S_l^2(\pi - \theta; 0) \right|^2 \right], \quad (3.25)$$

where the $\tilde{k}_{l2\omega P}$, defined as in Eq. (2.14), are numerically computed using the exact Schwarzschild radial equation and the $\tilde{k}_{l2\omega P}^{\text{Coul}}$ are obtained from (3.20) with the substitution $l \rightarrow \tilde{l}$. In fact, the summed Coulomb amplitude

$$g(\theta) = \sum_{l=2}^{\infty} \bar{k}_{l2\omega}^{Coul} S_l^2(\theta; 0)$$

is known²⁰ so we instead add to the numerically calculated result the summed Coulomb cross section and subtract the Coulomb contributions for $l \leq L$. We thus replace the first term in (3.25) by⁴

$$\frac{1}{h^2} \left| \sum_P \sum_{l=2}^L \left\{ \bar{k}_{l2\omega}^{Coul} - e^{i\bar{\alpha}} \frac{h[4\pi(2l+1)]^{1/2}}{2\omega} \times e^{i\eta_l} \sin \eta_l S_l^2(\theta; 0) \right\} + hg(\theta)e^{i\bar{\alpha}} \right|^2, \quad (3.26)$$

where $\bar{\alpha}$ is a constant necessary to reconcile the asymptotic constant difference between r^* and r_C^* . Typically $\bar{\alpha}$ is adjusted slightly so that the Coulomb and the calculated phases agree for $l=L$. This has the effect of strongly suppressing small-angle structure in the cross section. It of course completely eliminates any structure that arises from the $l > L$ phases.

For $a\omega \neq 0$ one still finds that the phase shifts approach the Coulomb values. If l is large then the angular eigenvalue E_l is approximately²³

$$E_l = l(l+1) - 2 \frac{ms^2 a\omega}{l(l+1)} - \frac{a^2 \omega^2}{2} + a\omega \sum_{n=1}^{\infty} \hat{P}_l(n), \quad (3.27)$$

where $\hat{P}_l(n)$ are successively higher-order corrections [of order $(a^2 \omega^2 / l^n)$] to the eigenvalues. Hence the condition for rapid convergence of the series to the Coulomb values requires only that $(a\omega)^2 / l < 1$. A similar requirement holds for approach of the Z_l^m to the spherical Y_l^m . Hence, even in the Kerr case, a replacement of the form (3.26) is valid.

For $|a\omega| < 2$, and $|M\omega| < 2.5$, $L \sim 20$ in Eq. (3.26) provides accuracy commensurate to the accuracy of the numerical integrations. (Matzner and Ryan⁴ had $L=10$.)

IV. RESULTS: ABSORPTION AND PHASES

We now examine the details seen in the calculated quantities. Our aim is to supply a physically intuitive context in which to understand the scattering phenomenon as a whole. To that end we first discuss in this section two simplified, physically analogous, problems: a square barrier and the null-torpedo model. Many features of the calculated cross sections may be understood with the aid of these simplified models.

A. Absorption

We may study the solution of the large- r limit of the radial equation in the form of Eq. (3.17)

by appealing to an analogous square-barrier problem. In the Schwarzschild case, the potential V_z in the perturbation equation (3.17) vanishes exponentially for negative r^* and varies as $r^{-2} \sim r^{*-2}$ for $r^* > 0$. In fact, the dominant terms in the potential are

$$V_l r^{-2} \simeq (dr/dr^*)l(l+1)/r^2. \quad (4.1)$$

The maximum of this term occurs (in Schwarzschild) at $r=3M$, and the potential may thus be approximated by a one-dimensional rectangular barrier in x with a potential of the form

$$V(x) = \frac{l(l+1)}{27M^2}, \quad -\frac{b}{2} < x < \frac{b}{2} \\ = 0, \quad \text{elsewhere} \quad (4.2)$$

for $-\infty < x < \infty$, where b is the classical turning point

$$b \simeq l/\omega. \quad (4.3)$$

Examining this simplified problem one finds intuitive explanations for much of the behavior of the absorption plotted in Figs. 1 and 2. For small l the energy of the wave $\sim \omega^2$ exceeds the height of the barrier and absorption is essentially complete so the ratio out/in is zero. As we consider larger l , the height of the barrier increases until it is comparable to the energy of the incoming wave and the transition is made to complete reflection. Since the simplified problem is exactly soluble the value of l at which the transition occurs may be estimated, and the onset of transmission is expected when $V \sim \omega^2$ or, using Eq. (4.2),

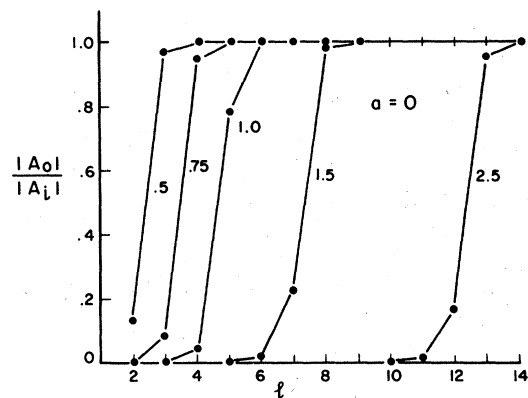


FIG. 1. The ratio of the magnitude of the amplitude A_0 of the scattered partial wave to the magnitude of the amplitude A_l of the same angular mode of the incoming wave as a function of l . Plots are shown for various values of frequency from $M\omega=0.5$ to $M\omega=2.5$ for Schwarzschild $a=0$. $|A_0/A_l|=0$ corresponds to complete absorption. $|A_0/A_l|=1$ corresponds to complete reflection. The numbers labeling each plot are the frequencies $M\omega$.

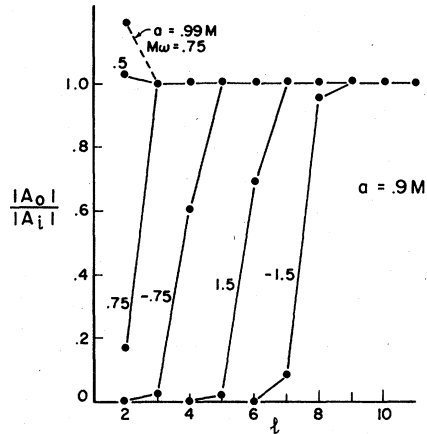


FIG. 2. The ratio of the magnitudes of the outgoing scattered to incoming amplitudes—as in Fig. 1—but for a Kerr hole with angular momentum given by $a = 0.9M$. The plots are again labeled by frequency $M\omega$. Negative frequency corresponds to counterrotation, positive frequency to corotation of the circular polarization with the hole. The dashed line at the top left is the plot for a nearly maximal Kerr hole with $a = 0.99M$ and $M\omega = 0.75$. Notice the superradiance shown for this case as well as for the $M\omega = 0.5$, $a = 0.9M$ case.

$$l(l+1) \sim 27M^2\omega^2. \quad (4.4)$$

This suggests the transition should occur around $l \sim 3$ or 4 for $M\omega = 0.75$ and near $l \sim 7$ or 8 for $M\omega = 1.5$.

Comparison with the calculated results displayed in Figs. 1 and 2 indicates reasonable agreement with the simplified problem. The transition occurs at $\omega \propto l$ for a given a/M , but the value of the constant of proportionality is a function of a/M . Further, the rapidity with which the transition occurs is consistent with the model. As l increases the transmission of the rectangular barrier decreases as

$$\exp(-2V^{1/2}b) \sim \exp[-2l^2/(3\sqrt{3}M\omega)]. \quad (4.5)$$

Although the approximation of the simple problem to the exact one is somewhat crude, one still expects a rapid transition from transmission to reflection as l increases and a sensitivity to small changes in the height of the potential barrier. These rough expectations are indeed fulfilled by the calculated values, although with modifications in detail due to the complicated nature of the exact potential.

The superradiance displayed in Fig. 2 for the low- l modes of the $M\omega = 0.5$, $a = 0.9M$ and the $M\omega = 0.75$, $a = 0.99M$ cases is unexpected from the simple classical models. It is unique to black-hole physics. The superradiance shown, with the smaller superradiance present in the $a = 0.9M$, $M\omega = 0.35$ case (not shown) is consistent with the

conclusions of Teukolsky and Press¹¹ that the amount of superradiance increases as $\omega \rightarrow \omega_s = am/2Mr$, and cuts off abruptly as $\omega = \omega_s$. As later discussion in this chapter will show, this enhancement of the lower l modes increases the scattering in the backward direction since the low- l modes (low angular momentum) scatter to larger angles.

There is another way of viewing the variation of absorption with l . One may view each l mode as an incident null trajectory with an impact parameter b given by

$$b\omega \approx E_l^{1/2} \sim [l(l+1)]^{1/2} \quad (4.6)$$

as discussed in Sec. III (see Fig. 3). Choose a fixed value of a . One then expects that the maximum b for which significant absorption occurs would correspond to those trajectories incident parallel to the angular momentum of the hole which are marginally trapped by the hole. As ω increases the value of l corresponding to the impact parameter of the marginally bound trajectory also increases. In fact, if the value of l at which absorption drops off is taken from Fig. 1 for Schwarzschild as $l_0 = 3, 4,$ and 7 for $M\omega = 0.75, 0.1,$ and 1.5 , respectively, the resultant average apparent size of the Schwarzschild hole is $b \sim 5.2M$ which is (probably somewhat coincidentally) the exact result from solution²⁴ of the geodesic equation $3^{3/2}M = 5.2M$.

With this point of view, the split in l values at transition from absorption to reflection in Fig. 2, between the corotating and the counterrotating circular polarization cases in Kerr, is interesting. If this procedure

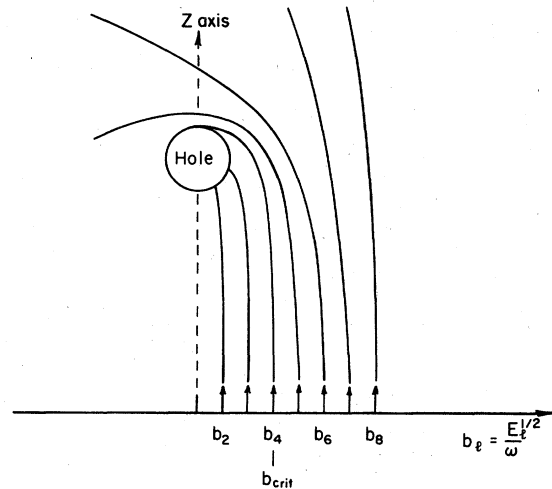


FIG. 3. A battery of null torpedoes is (arrows at bottom) incident parallel to the z axis of the hole. Spacing between the torpedoes is $(E_{l+1}^{1/2} - E_l^{1/2})/\omega \sim 1/\omega$. See the text for a discussion.

constitutes a numerical estimate of the apparent size of the Kerr hole as viewed along the rotation axis then using the data in the figures the average respective sizes become, for $a=0.9M$, $b_+ \sim 3.7M$ for the corotating $\omega > 0$ case and $b_- \sim 5.6M$ for the counterrotating $\omega < 0$ case. This suggests that if one were to solve for the marginally trapped null geodesics with incident direction parallel to the axis of the rotation of the hole one should expect a splitting in the apparent size of the hole depending on whether the angular momentum of the hole and spin angular momentum of the incoming wave were aligned or not, with the minimal apparent size corresponding to the case of greatest total angular momentum in the ϕ direction.

If, instead, one estimates the apparent size of the hole from total absorption cross sections calculation via Eq. (2.13), a splitting is still evident between corotating and counterrotating incident waves. For instance, for $a=0.9M$ and $|M\omega| = 1.5$, one finds $\sigma_{\text{abs}} = 80.3M^2$ for counterrotating and $\sigma = 62.5M^2$ for corotating incident waves. By $\sigma_{\text{abs}} = \pi \bar{b}^2$ this gives $\bar{b}_- = 5.06M$ and $\bar{b}_+ = 4.46M$. The Schwarzschild numerically calculated value for $M\omega = 1.5$ is $\bar{b}_{\text{Sch}} = 5.15M$, indicating that the geometrical optics absorption behavior (corresponding to $\bar{b}_{\text{Sch}} \sim 5.2M$) has not been reached for the relatively low frequency $M\omega = 1.5$.

B. Phases

The simplified rectangular-barrier problem of Eq. (4.2) is also useful in understanding the behavior of the phase of the scattered wave (equivalent in the case of zero absorption to the usual phase shift). Figures 4–7 display the computed phases versus l , for $a=0.9M$, $M\omega = \pm 0.75$, and $M\omega = \pm 1.5$. Figure 8 shows the phase for the corotating case $M\omega = 0.75$, $a = 0.99M$. For small values of l the phase is uniformly $-\pi/2$. Since the outgoing-plane-wave amplitude is proportional to i [see Eq. (2.9) and the Appendix] a phase of $-\pi/2$ indicates total absorption since the corresponding term in the scattering amplitude is then just the negative of the plane-wave part. As l increases the scattering enters the region of transition between total absorption and reflection and the phases are relatively erratic. In the rectangular-barrier problem, the reflection amplitude when absorption is substantial is

$$R \approx i \exp(-2i\omega b) \quad (4.7)$$

$$\approx i \exp[-2i(l^2 + l)^{1/2}].$$

Hence the phase is $\sim [l(l+1)]^{1/2}$. Since the phase is modulo 2π this gives the erratic behavior of the phases in the transition region. We emphasize that the magnitude of the outgoing wave in these

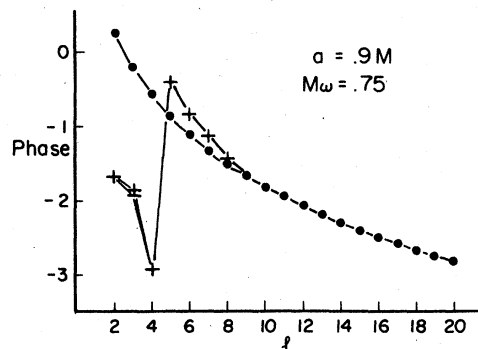


FIG. 4. This figure, along with Figs. 5–8 immediately following, shows the phase of the scattered waves for various frequencies for $m=+2$. The $m=-2$ case may be obtained via the reality condition $\bar{K}_{l,m\omega P} = PK_{l-m-\omega P}$. The phases of positive-parity $P=+1$ waves are shown with pluses. Minuses indicate the negative-parity phases where they are significantly different. Coulomb phases are shown as dots. As discussed in the text, waves which are completely absorbed possess the phase $-\pi/2$. For the case shown here, $a=0.9M$ and corotating frequency $M\omega=0.75$, the phase for only the lowest $l=2$ mode shows nearly complete absorption (phase $=-\pi/2$). Between $l=3$ and $l=5$ the phase changes rapidly, yielding a large value of the semiclassical deflection function $\Theta(l) = 2d(\text{phase})/dl$. This suggests large-angle scattering for these modes. For $l \geq 5$ the Kerr phases approach the Coulomb values rapidly, being virtually identical for $l \geq 8$.

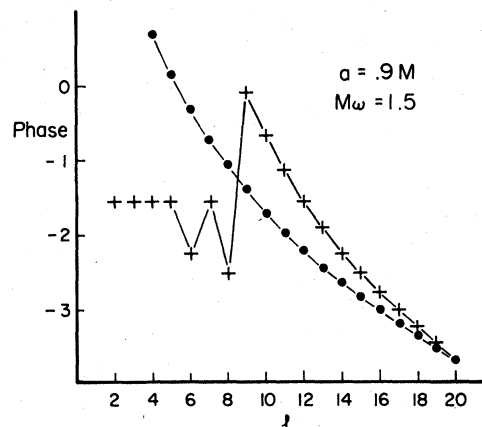


FIG. 5. This plot is similar to Fig. 4 but for $a=0.9M$, $M\omega=1.5$. Notice the larger region for low l (between $l=2$ and $l=4$) showing complete absorption. Notice also that the region between complete absorption and approach to the Coulomb values is much larger in l . This, plus the fact that the phases are changing erratically there, leads to a semiclassical expectation of greater interference between modes in the large-angle scattering features. The Kerr phases do not become nearly equal to the Coulomb phases until $l \sim 20$; in fact, integration to even higher l values would be necessary to completely determine the asymptotic l behavior of the phase.

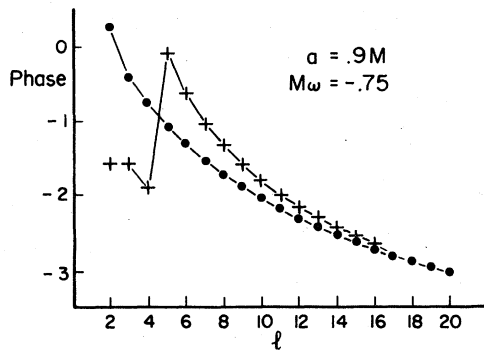


FIG. 6. This is a plot of the phases similar to Fig. 4 but for counterrotation $a = 0.9M$, $M\omega = -0.75$. In comparison to the corotating case of Fig. 4, notice that this case shows more complete absorption for the low l modes and only one or two modes which have phases differing greatly from neighboring modes. As discussed in the text this implies less oscillation in the cross sections at large angles since fewer modes participate in large-angle scattering, resulting in less interference. Finally, notice that the counterrotating case approaches the Coulomb phases more slowly than the corotating case of the same frequency. These features are even more apparent at larger frequency (see Fig. 7).

cases is small.

As l increases into the region of greater reflection, the figures show a convergence to the Coulomb value. The convergence is slower in l for larger values of $a\omega$, indicating that even for the relatively small value $M\omega = 0.75$ one should compute phase shifts for l past 10 (the value to which Matzner and Ryan⁴ were limited) to obtain the details of the cross sections. The truncation to l

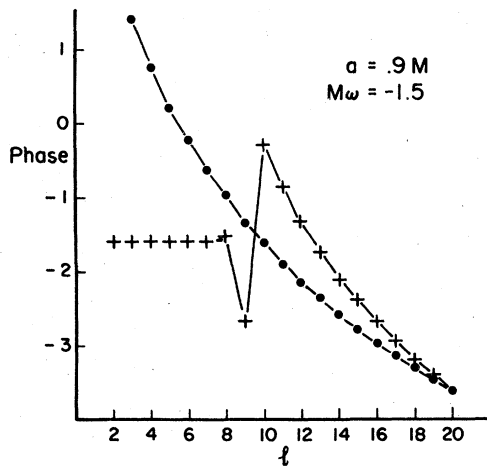


FIG. 7. This is the counterrotating $a = 0.9M$, $M\omega = -1.5$ case corresponding to Fig. 5. The comments of Fig. 6 apply here as well, but this example is even more striking than the lower-frequency case. Compare this figure with Fig. 5.

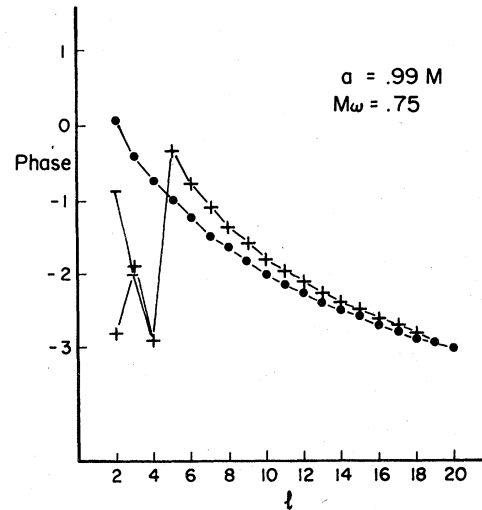


FIG. 8. This figure shows the phases for the highly superradiant, nearly maximal, Kerr case, $a = 0.99M$, $M\omega = 0.75$. It should be compared to Figs. 4 and 6. Notice that the $l = 2$ mode not only is not strongly absorbed but shows a large difference in phase between the positive- and negative-parity waves. This leads to a large backward contribution as discussed in the text. The intermediate modes, between $l = 3$ and $l = 6$, are very similar to the $a = 0.9M$, $M\omega = 0.75$ case whereas the large l modes appear similar to the counterrotating $M\omega = -0.75$ case. Thus we expect a large-angle interference pattern similar to that of the counterrotating case, with similar angular behavior of the maxima and minima, but a large background backward contribution due to the superradiance in the lowest two modes. This is seen in the cross sections in Fig. 14.

$= 10$ in the calculated cross sections of Matzner and Ryan and the resultant normalization to the Coulomb value at $l = 10$ suppresses (at least) the interference pattern expected between the higher l modes. This should be particularly evident for the higher values of $a\omega$. [See also the discussion after Eq. (3.26) above.]

(The calculations here extend only up to $a\omega = 1.35$ ($a = 0.9M$, $M\omega = 1.5$) for which the value $L = 20$ [cf. Eq. (3.26)] is sufficient. It should be observed that this limitation is not imposed by the radial integration since the integration of the radial equation via the JWKB approximation becomes more efficient as l increases. Instead the limitation was imposed by the necessary solution of the angular equation (A1) for the ${}_sS_l^m$ and ${}_sE_l^m$. The technique used here is exactly that of Press and Teukolsky,¹⁷ namely, a continuation method based on an expansion for the spheroidal functions ($a\omega \neq 0$) in terms of the spherical functions ($a\omega = 0$). Integration of the continuation equation to large values of $a\omega$ is a relatively time-consuming process. Other techniques, such as a modified JWKB procedure for the large- l angular functions, would alleviate this

difficulty, but we have not attempted such an analysis.)

We mentioned in Sec. II that our approach gives the parity dependence of the calculated scattered wave in a direct way, since the nontrivial parity dependence appears only in the incoming plane Riemann-tensor wave. The importance of the parity dependence of the phase shifts lies in its implication for significant backward scattering. For any value of l a backward contribution to the cross section arises only from the second absolute square term in Eq. (3.25) since the ${}_2S_m^2(\theta)$ vanish at $\theta = \pi$ but not at $\theta = 0$.¹³ Hence a backward contribution is found only when

$$\bar{k}_{l2\omega P=1} - \bar{k}_{l2\omega P=-1} \neq 0; \quad (4.8)$$

in other words, when the difference in phase shifts between the two parities is significant. Any difference in phase arises from the parity dependence of the asymptotic plane wave $\sim \text{Re}C + 12iM\omega P$. Since $\text{Re}C \sim (E_l)^2$, the phase splitting in parity is

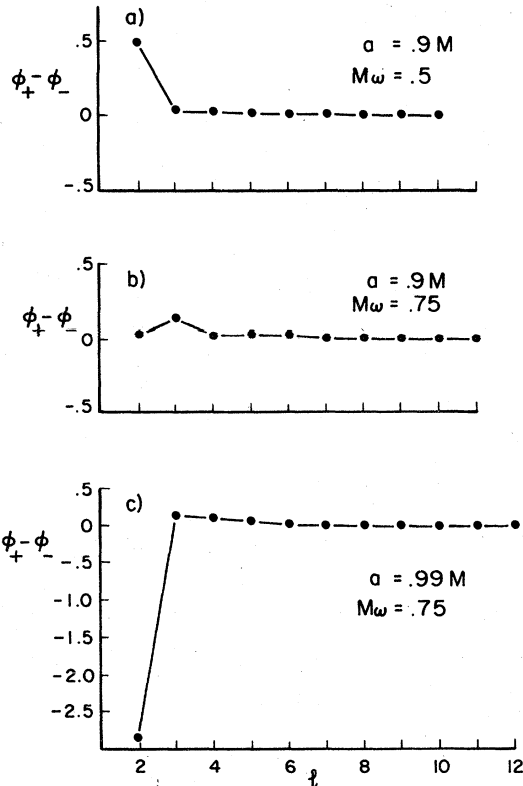


FIG. 9. The difference $\phi_+ - \phi_-$ between the positive-parity $P=+1$ and the negative-parity $P=-1$ phases for Kerr holes with several values of frequency $M\omega$ and a . The difference between the phases is important for understanding the backward ($\theta \sim \pi$) behavior of the cross sections as discussed in the text. These plots are illustrative of the cases in which the difference is significant.

maximal for smaller values of l . At the same time, for the phase splitting to contribute to the backward scattering, the mode concerned must not be substantially absorbed. Therefore we expect the maximal phase splitting, hence maximal backscattering, to occur for smaller corotating frequencies and larger values of a , particularly those values for which there is considerable superradiance.

Using the potential of Eq. (4.2) we may estimate the maximum frequency for significant phase splitting as that value of ω which has ω^2 comparable to the maximum height of the potential for small l , i. e., $M^2\omega_{\text{max}}^2 \sim (2 \times 3)/27$ providing

$$M\omega_{\text{max}} \sim 0.5. \quad (4.9)$$

Figure 9 illustrates the difference in phases for several cases in which it was significant, $a=0.99M$, $M\omega=0.75$; and $a=0.9M$, $M\omega=0.75$ and 0.5 . Frequencies lower than those estimated via (4.9) above also show phase splitting⁴ but as frequency increases for a given value of a , absorption quickly becomes complete at small l values. The large phase splitting for $a=0.99M$ is particularly significant for backward scattering since this case shows large ($\sim 120\%$) superradiance in the phase split $l=2$ mode (see Fig. 2). The resultant significant backward scattering is evidenced in the angular cross sections discussed in Sec. VI.

Since parity splitting in phase appears explicitly in the plane-wave expression the l dependence of the resultant splitting may be determined. Using the explicit parity dependence of the incident plane waves, one finds the resultant phase term given by

$$\begin{aligned} \bar{k}_{l2\omega P=+1} - \bar{k}_{l2\omega P=-1} &= \bar{k}_{l2\omega P=+1} \frac{24iM\omega}{[(\text{Re}C)^2 + 144M^2\omega^2]^{1/2}} \\ &\times \exp\left[-i \tan^{-1}\left(\frac{12M\omega}{\text{Re}C}\right)\right]. \end{aligned} \quad (4.10)$$

For large l , $\bar{k} \rightarrow \bar{k}^{\text{Cou}l}$ and

$\text{Re}C \rightarrow \text{Re}C(\text{Schwarzschild})$

$$= l(l+1)(l+2)(l-1) \gg 12M\omega. \quad (4.11)$$

Hence, for large l the parity-split term is

$$\begin{aligned} \sum_P P \bar{k}_{l2\omega P} &\xrightarrow{\text{large } l} \bar{k}^{\text{Cou}l} \frac{24iM\omega}{l(l+1)(l+2)(l-1)} \\ &\propto \bar{k}^{\text{Cou}l} l^{-4}. \end{aligned} \quad (4.12)$$

For $l \geq 20$ the relative contribution to the scattering from the large- l modes is less than one part in 10^6 and virtually no contribution to the cross section is lost by truncating the computations as we do, at $L=20$.

V. SEMICLASSICAL DESCRIPTION OF SCATTERING

A substantial gain in understanding the results computed here can be achieved by considering a modified JWKB-wave-mechanics description which allows a direct connection between the phases, say, the classical deflection angle [Eq. (5.2) below], and the classical cross section. This section is named after the definitive reference on the subject: Ford and Wheeler.²⁵ Almost all the qualitative features of the scattering can be understood by appealing to the semiclassical analysis, a fact which greatly enhances our confidence in the numerically computed results. The principal difference between Ford and Wheeler's treatment and ours is that they considered only elastic scattering. For black holes, we know, and Figs. 1 and 2 confirm, that absorption and superradiance are also important phenomena, as is phase splitting (Fig. 9). We shall see that in some situations they make significant modifications to the cross section expected from the Ford-Wheeler analysis.

The JWKB analysis of a quantum-mechanical short-range real (spherically symmetric) potential scattering problem yields phase shifts [analogous to the η_l of Eq. (3.19) but note that the ordinary Euclidean radial variable r would appear in the short-range-potential form of that equation]:

$$\delta_l = \pi/4 + l\pi/2 - k r_0 + \int_{r_0}^{\infty} (k_r - k) dr, \quad (5.1)$$

where $k = 2\pi/\lambda$, $k_r = [2\mu\hbar^{-2}(E - V) - (l + \frac{1}{2})^2 r^{-2}]^{1/2}$, μ is the mass of the scattered particles, and r_0 is the classical turning radius of the orbit of energy E . The centrifugal barrier is changed from its quantum form $r^{-2}l(l+1)$ to $r^{-2}(l + \frac{1}{2})^2$, a standard technique to improve the accuracy of semiclassical calculations.²⁶ By comparison to the orbital equation for *classical* motion in the potential V we see that the classical deflection function $\Theta(l)$ is

$$\Theta(l) = 2d\delta_l/dl. \quad (5.2)$$

Hence, a knowledge of the JWKB phase shift can be expected to predict the qualitative behavior of the cross section, via the classical formula

$$\left. \frac{d\sigma}{d\Omega} \right|_{\text{classical}} = \left| \frac{b}{\sin\Theta} \frac{db}{d\Theta} \right| \quad (5.3a)$$

$$= \frac{\omega^{-2}(l_{\text{cl}} + \frac{1}{2})}{|\sin\Theta|} \left| \frac{d\Theta}{dl} \right|^{-1}. \quad (5.3b)$$

Two classical scattering phenomena have important analogs in black-hole scattering. The first is *glory* scattering. This arises when the deflection function passes smoothly through 0, or $\pm\pi$, etc. Classically, the vanishing of $\sin\Theta(l)$ where $d\Theta/dl$ is finite leads to a singularity in the cross section for forward or backward scattering.

This effect can certainly arise in the black-hole case. The forward divergence of the Coulomb problem can be viewed as a forward glory. In the black-hole case the possibility of deflection via spiralling orbits that wrap a large number of times is also a possibility, so we expect *backward* glories in the black-hole case.

Following Ford and Wheeler, consider a backward glory. Then

$$\Theta(l) \approx \pi + a(l - l_g), \quad (5.4)$$

where l_g is the angular momentum corresponding to the $\Theta = \pi$ orbit. From (5.4) and (5.3) we see that $d\sigma/d\Omega|_{\text{classical}} \sim 1/|\Theta - \pi|$. Equation (5.4), with (5.2), leads to

$$\delta_l = \frac{\pi}{2}(l - l_g) + \frac{1}{4}a(l - l_g)^2 + \delta_g, \quad (5.5)$$

where δ_g is the glory phase shift, corresponding to $\Theta = \pi$. The usual expression for the scalar scattering amplitude (except in the forward direction; cf. Landau and Lifshitz²⁷)

$$f(\theta) = \frac{\lambda}{4\pi i} \sum_{l=0}^{\infty} (2l+1) e^{2i\delta_l} P_l(\cos\theta) \quad (5.6)$$

may be approximated by an integral, and the $\cos\theta \approx -1$ behavior of P_l may be approximated as a Bessel function

$$f(\theta) \approx \frac{\lambda}{4i\pi} e^{2i\delta_g} e^{-\pi i l_g} \times \int_0^{\infty} (2l+1) e^{ia(l-l_g)^2/2} J_0(l \sin\theta) dl. \quad (5.7)$$

The integral may be approximately evaluated²⁵

$$f(\theta) \approx \frac{\lambda l_g (2\pi)^{1/2}}{2\pi(a)} e^{i(2\delta_g - \pi l_g - \pi/4)} J_0(l_g \sin\theta), \quad (5.8)$$

where this approximation now neglects the difference between l_g and $l_g + \frac{1}{2}$. The cross section in the backward direction is thus proportional to

$$J_0^2(l_g \sin\theta). \quad (5.9)$$

The singularity in the classical cross section is replaced by a finite peak. When the Bessel function is averaged over several cycles $\langle J_0^2(x) \rangle = 1/\pi x$, the classical result is recovered.

If more than one value of l leads to $\Theta = \pi$ deflection, then the amplitudes add; this may lead to phase interference between the amplitudes with different l_g .

The second important semiclassical phenomenon is so-called "orbiting" scattering. In quantum mechanics this occurs because the effective potential (i. e., including the centrifugal term) has a local maximum. The behavior of the deflection function, for an energy just at the value of the

local maximum, is, according to Ford and Wheeler

$$\Theta(l) = \theta_1 + b \ln\left(\frac{l-l_1}{l_1}\right), \quad l > l_1 \quad (5.10a)$$

$$\Theta(l) = \theta_2 + 2b \ln\left(\frac{l_1-l}{l_1}\right), \quad l < l_1 \quad (5.10b)$$

where b , θ_1 , and θ_2 are constants, and l_1 is the value of l which satisfies

$$V_{\text{effective}}(r_1, l_1) = E, \quad (5.11)$$

where r_1 is the radius at which the maximum in $V_{\text{effective}}$ occurs. It is possible that the logarithmic variation in Θ occurs in an angular momentum interval $\Delta l < 1$. A logarithmic excursion in $\Theta(l)$ over such an interval requires that δ_l have extremely large derivative—is essentially discontinuous—over this interval. As Ford and Wheeler show, this effect can lead to a dip in the cross section at the angle $\Theta(l_1)$ (Fig. 10). We should expect *qualitative* features of the glory or orbiting type in black-hole scattering, but differences certainly exist, especially because there is absorption by black holes. We will also find effects specifically due to the polarization of the gravitational waves which modify the semiclassical scalar analysis of this section.

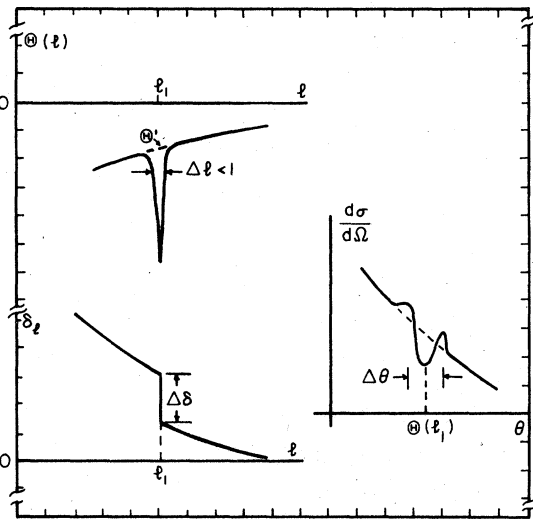


FIG. 10. An illustration of a sharp orbital dip from Ford and Wheeler (Ref. 25). The sharp discontinuity $\Delta\delta_l$ in the phase shift δ_l at l_1 leads to a deep minimum in the deflection function $\Theta(l)$ at l_1 . The characteristic orbital dip then appears at $\theta = \Theta'(l_1)$ where $\Theta'(l)$ is the smoothed deflection function ignoring the discontinuity in δ_l . The angular width of the orbital dip is $\delta\theta \sim [d\Theta'/dl]_{l_1}^{-1/2}$. Compare the characteristic shape of the orbital dip with the features seen in the Kerr cross sections of Figs. 13 and 14.

There is a third semiclassical quantum-scattering effect, namely, rainbow scattering. This occurs if $d\Theta/dl$ vanishes. Since the deflection (at least for Schwarzschild black holes) always increases as l decreases, this phenomenon strictly does not occur in scattering by black holes. However, the glory phenomenon can be viewed as behavior of this type for $\Theta = \pi$, $\Theta = 0$ scattering, since $\Theta = \pi + \epsilon$, $\Theta = \pi - \epsilon$ (for instance) are not distinguishable. Rainbowlike behavior will thus be expected (see Figs. 12–14) because different frequencies are scattered differently.

VI. RESULTS: CROSS SECTIONS

Figures 11–13 display cross sections chosen because they display typical qualitative structure of the kind suggested by the semiclassical discussion of the preceding section. Figures 11 and 12 are calculated for a nonrotating black hole. These figures define a baseline against which to measure the considerably more intricate Kerr cases displayed in Fig. 13.

The feature which all these cross sections have—*must* have—in common is a forward Coulomb peak $\sim \theta^{-4}$. For a given frequency, the angular momentum can be chosen so large than the geometrical optics result of the Einstein deflection

$$\Theta(l) \approx 4M/l\omega$$

holds; this leads directly to the Coulomb divergence.

The overall Coulomb behavior is, however, significantly modified by glory and orbiting scattering. Figure 11 shows the Schwarzschild cross section for fairly low frequency ($M\omega = 0.1$).⁴ Besides the Coulomb behavior, there is some backward enhancement since at this frequency there is no absorption for any l but some parity splitting of the behavior of $l=2$ phase shifts. In the limit $\omega \rightarrow 0$, the backward scattering vanishes.²⁰ The $M\omega = 0.75$ case in Fig. 12 begins to evidence the features predicted by the semiquantitative analysis of Sec. V, although considerable intuition is required to recognize the emergence of the glory in the backward quadrant. Near clairvoyance is required to view the dips below $\theta = \pi/2$ as orbital dips. (But compare this and the following Schwarzschild cases to the Kerr cross sections which show enhanced orbital dips.) The significantly reduced scattering in the backward direction evidences the substantial absorption of low- l modes. The total absorption cross section of the hole at this frequency is $72.4M^2$ corresponding to a capture radius of $b = 4.8M$.

The Schwarzschild cross sections in Fig. 12 for

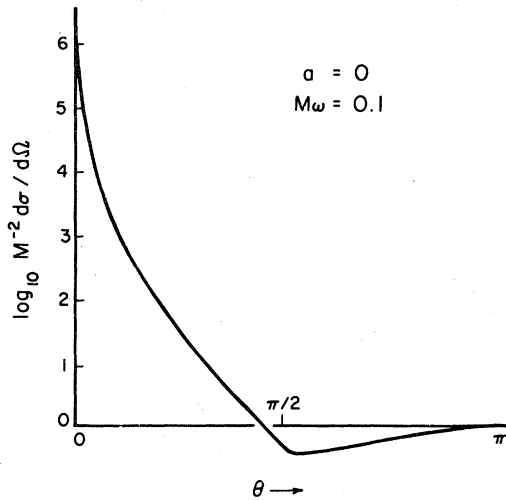


FIG. 11. The differential cross section as a function of angle for Schwarzschild with $M\omega=0.1$, from Matzner and Ryan (Ref. 4). This plot presents the low-frequency scattering cross section. Notice the Newtonian-type behavior at all angles, especially the lack of significant backward scattering. The exact Newtonian situation has exactly vanishing backward scattering. This is due to nearly complete reflection of all low l modes, with only slight phase splitting. Compare this plot with the higher-frequency cross sections in Fig. 12 immediately following.

$M\omega=1.5$ and 2.5 give clear evidence of the Bessel-function oscillations characteristic of glory scattering. Progressing to smaller angles from near $\theta=\pi$, the regular glory oscillations give way to the somewhat washed out orbital dip near $\pi/2$.

Notice that as frequency (and hence absorption) increases, the depth of the backward cross section minimum increases, and the glory crowds closer to π . The backward minimum is a polarization effect; backward scattering requires a difference with parity of a nonabsorbed l mode. (Notice that parity affects only phase, not absorption.) The glory can be related to the first nonabsorbed l . Glory—and orbiting—phenomena occur for spiraling orbits that penetrate very close to the black hole; the next smaller value of angular momentum would lead to total absorption. From Fig. 1 we expect $l_g \sim 8$ and 14 , respectively, for $M\omega=1.5$ and 2.5 . Indeed, the angular separations of the glory minima correspond closely to these values.

The calculated absorption cross sections for $M\omega=1.5$ and $M\omega=2.5$ are $83.36M^2$ and $83.61M^2$, respectively, corresponding to minimal impact parameters $b=5.15M$ and $5.16M$. This compares well with the analytical Schwarzschild geometrical-optics value of $5.2M$.

The general features seen in the Schwarzschild cross sections are then clear. In the forward

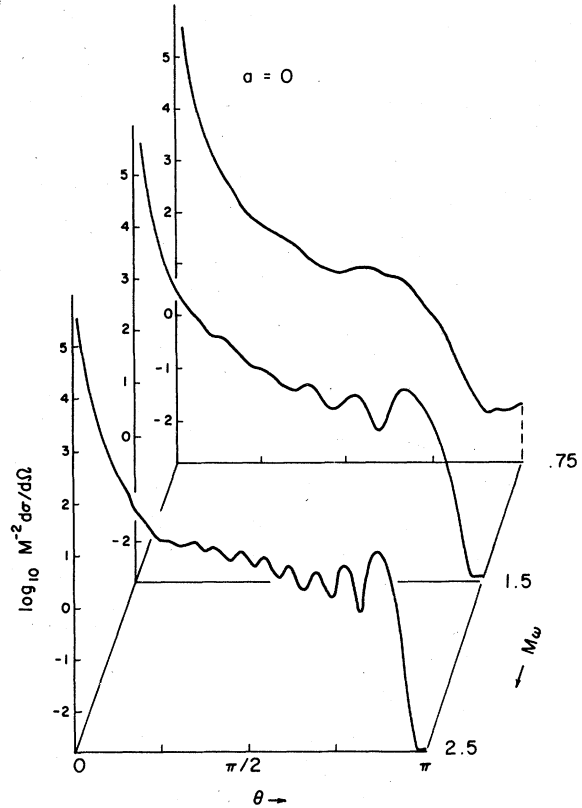


FIG. 12. Calculated differential cross sections for Schwarzschild for several values of $M\omega$. These cross sections were computed as described in the text by summing the numerically obtained amplitudes from $l=2$ to $l=20$ and adding the transcribed Coulomb amplitude for the remaining l modes. Notice the striking emergence of the backward glory as frequency increases. The oscillatory section has the Bessel-function behavior characteristic of glory scattering. Notice also the deep backward minimum due to increased absorption of the low l modes at higher frequencies.

direction one finds a Coulomb divergence falling off as θ^{-4} , giving way to at least one somewhat subdued orbital dip in the vicinity of $\theta=\pi/2$. If the cross sections for $M\omega=0.75$, 1.5 , and 2.5 are overlaid another orbital dip at $\theta \sim \pi/3$ appears to occur at very nearly the same angle. A pronounced glory is seen; its characteristic Bessel-function behavior occurs closer to the backward direction as frequency increases. A deep minimum in the backward direction becomes sharper and deeper as frequency increases. Finally, as the frequency increases the total absorption cross section approaches the analytical value $27\pi M^2$.

Examination of the Kerr cross sections in Fig. 13 reveals the same general structure with interesting peculiar complications. Consider first the corotating case, $a=0.9M$, $M\omega=+0.75$. Apart

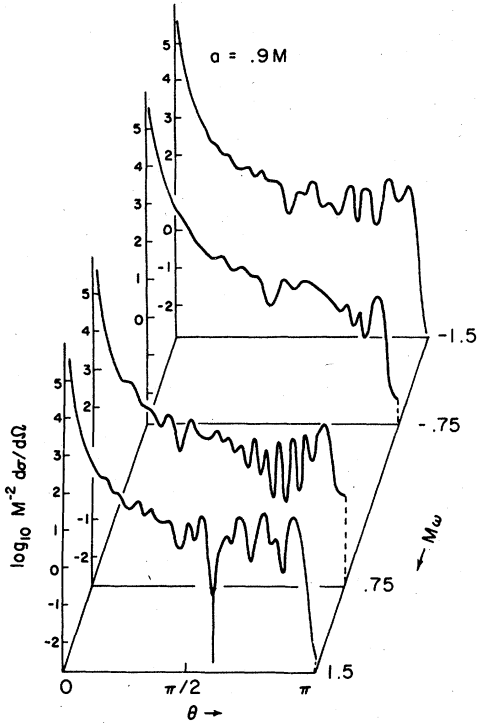


FIG. 13. This figure displays differential scattering cross sections for a Kerr hole with $a=0.9M$ for various values of incident frequency $M\omega$. Each shows the characteristic backward glory near $\theta=\pi$ but notice the enhanced oscillation in the corotating positive $M\omega$ cases due to reduced absorption of the low l modes. The orbital features are distinct in all cases as a fairly pronounced dip typically just below $\theta\sim\pi/2$ and a smaller dip near $\theta\sim\pi/4$. For a given value of $|M\omega|$ the dips occur at smaller angles for the case of corotation. The source of the peculiar deep narrow dip at $\theta=0.612\pi$ in the $M\omega=1.5$ case is obscure. The orbital dips seen here should be compared to the generic case shown in Fig. 14. Some suppression of very fine angular scale ($l>20$) has probably been imposed by the Coulomb normalization of the phases for $|M\omega|=1.5$ (cf. Figs. 5 and 7).

from the Coulomb forward divergence a pronounced orbital dip appears again around $\theta=\pi/3$ followed by either secondary dips or interference due to the same disturbance. The angular width of the pronounced dip correlates well with the value of $\delta\theta\sim[d\theta_{\text{Coul}}/dl]^{1/2}$ expected from the analysis of Ford and Wheeler. The glory near $\theta=\pi$ displays a beautiful oscillatory behavior. In the backward direction the minimum is evident but significantly more subdued than the corresponding Schwarzschild case, due to the relatively slight absorption in Kerr at this co-rotating frequency. The total absorption cross section in this case is only $36.5M^2$ corresponding to $b=3.41M$.

Compare this cross section to the $a=0.9M$, $M\omega=+1.5$ (also corotating) case which is also plotted

in Fig. 13. The orbital dip at $\theta\sim\pi/3$ is significantly modified probably due to an increased tendency for absorption while the dip closer to $\theta=\pi/2$ appears more prominent in this case. The glory occurs at nearly the same angle as the $M\omega=0.75$ case but the oscillatory behavior is considerably more complicated due possibly to interference with orbital features. A feature unique to this case is the peculiar extremely deep and narrow dip at $\theta=0.612\pi$ of width $\delta\theta\leq 0.015\pi$. Its origin is uncertain but it may be an orbital feature corresponding to the larger values of l where $d\theta/dl$ is smaller. The total absorption cross section in this case is $62.5M^2$ corresponding to $b=4.46M$. This produces the deep minimum in the direct backward direction since the small- l modes which otherwise produce backward scattering are absorbed.

For significant a , the cross sections for the counter-rotating case show considerably weaker features. Figures 4–8 show that the counterrotating case possesses a narrower range in l of strongly varying phase shifts than does the corotating cases with the same $|M\omega|$. We therefore expect fewer particular l values to contribute to the striking “semiclassical features” apparent in the other cross sections.

The counterrotating $a=0.9M$, $M\omega=-0.75$ is plotted in Fig. 13 with the cross sections already discussed. A pronounced orbital dip is evidenced for $\theta\approx\pi/2$, and a secondary dip occurs at $\theta\approx\pi/3$ where the corotating case $M\omega=+0.75$ also possesses a dip. The glory is considerably less glorious in the counterrotating case but comparison to the corotating glory shows the positions of the maxima and minima are the same in the two cases. The backward minimum is deeper than in the corotating case since the counterrotating total absorption cross section is $88.7M^2$, corresponding to $b=5.31$, very nearly the same as the Schwarzschild case, and much larger than the corotating absorption.

The forward features of the counterrotating $a=0.9M$, $M\omega=-1.5$ case also plotted in Fig. 13 are nearly a carbon copy of the corotating case. The glory is considerably less oscillatory and there is no evidence of the sharp narrow dip of the corotating case. The backward minimum drops to virtually zero scattering. In this case the absorption cross section is $80.3M^2$ corresponding to $b=5.06M$.

Finally, Fig. 14 shows the nearly maximal Kerr case $a=0.99M$, $M\omega=0.75$, for which superradiance is definitely significant. The most prominent feature of the cross section is the dramatic enhancement of backward scattering. This feature arises from the large superradiance which en-

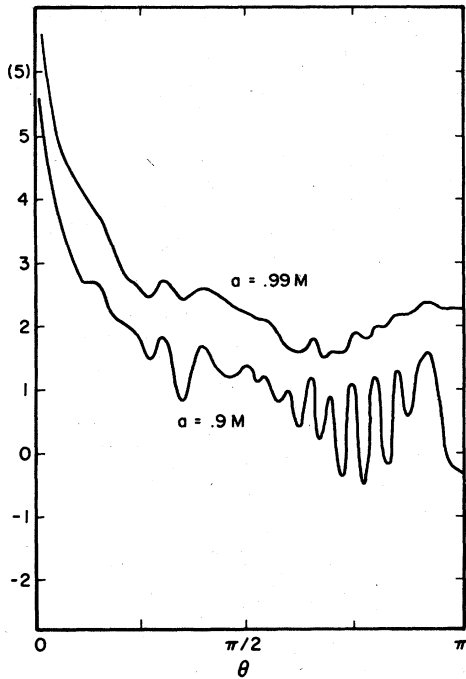


FIG. 14. Two differential cross sections as a function of θ , displaying the effect of superradiance. Both curves are for an incident frequency of $M\omega=0.75$. The lower curve is for a hole with $a=0.9M$ for which superradiance is relatively small. The upper curve is for the nearly maximally rotating case $a=0.99M$ with large superradiance. The latter curve has been displaced upward by a factor of 10 (+1 on the logarithmic scale) for clarity. The value $\log_{10}(M^{-2}d\sigma/d\Omega)=5$ in parentheses corresponds to the upper curve only and sets the scale for that plot. Notice the coincidence of the angles at which the maxima and minima occur in the two cases. Notice also that the oscillatory behavior in the backward direction is more pronounced in the nonsuperradiant case, $a=0.9M$.

hances the lowest l (parity-split modes). The total absorption cross section in this case is in fact negative ($-15.8M^2$). In the absence of the previous calculations one would hesitate to interpret the angular features of Fig. 14. But when the $a=0.9M$, $M\omega=0.75$ case in Fig. 13 is overlaid on Fig. 14 the structure is clear: Each of the maxima and minima in the almost maximal Kerr case corresponds to a maximum or minimum in the $a=0.9M$ case. Further, the amplitudes of the maxima are very nearly equal in the two cases. The superradiance has the effect of imposing a large background over the pattern, filling in the interference minima; the glory in the $a=0.9M$ case appears as barely a dimple on the superradiant scattering. But once the background is taken account of, the features in the two cases are essentially identical.

VII. CONCLUSION

We have investigated a number of cross sections for gravitational radiation scattering off a vacuum black hole. A number of explicit examples result, displaying the phenomena predicted by a semiclassical analysis. It remains to extend the catalog of Matzner and Ryan⁴ via the techniques developed here. This may require some further investigation of the integration of the angular equation, but should present no real difficulty. After that one may investigate off-axis scattering in the Kerr geometry. The most important result of the present work is the realization that semiclassical analysis and intuition can explain, if not predict, much of the structure of gravitational scattering cross sections.

ACKNOWLEDGMENTS

It is a pleasure to thank Professor J. A. Wheeler for many stimulating conversations. This work was supported in part by National Science Foundation Grant No. PHY77-07619.

APPENDIX A: DEFINITIONS AND USEFUL RELATIONS

The angular part of the separated perturbation variable

$$\Psi_{(s)} = e^{-i\omega t} e^{im\phi} {}_s S_l^m(\theta; a\omega) R_{l,m}(r, \omega)$$

obeys

$$\frac{1}{\sin\theta} \frac{d}{d\theta} \left(\sin\theta \frac{dS}{d\theta} \right) + \left(a^2 \omega^2 \cos^2\theta - \frac{m^2}{\sin^2\theta} - 2ms \frac{\cos\theta}{\sin^2\theta} - 2a\omega s \cos\theta - s^2 \cot^2\theta + s + E \right) S = 0. \quad (\text{A1})$$

The solutions to the radial and angular Teukolsky equations (2.3) and (A1) of $s=+2$ and $s=-2$ are related by the differential equations

$$\mathcal{D}\mathcal{D}\mathcal{D}\mathcal{D}_{-2}R = \frac{1}{4} {}_{+2}R \quad (\text{A2})$$

and

$$\mathcal{L}_{-1}\mathcal{L}_0\mathcal{L}_1\mathcal{L}_2 {}_2Z = (\text{Re}C) {}_2Z, \quad (\text{A3})$$

where

$$\mathcal{D} = \partial_r - i[(r^2 + a^2)\omega - am]/\Delta \quad (\text{A4})$$

and

$$\mathcal{L}_n = \partial_\theta + m \csc\theta - a\omega \sin\theta + n \cot\theta. \quad (\text{A5})$$

The constant C of Sec. II is given by

$$\begin{aligned} (\text{Re}C)^2 = & (Q^2 + 4am\omega - 4a^2\omega^2)[(Q-2)^2 \\ & + 36a\omega m - 36a^2\omega^2] \\ & + 2(Q-1)(96a^2\omega^2 - 48a\omega m) - 144a^2\omega^2, \end{aligned} \quad (\text{A6})$$

$$\text{Im}C = 12M\omega \quad \text{with } Q = {}_s E_l^m + a^2\omega^2 - 2a\omega m.$$

The angular equation admits among the ${}_s S_l^m$ the symmetries

$${}_s S_l^m(\theta; a\omega) = (-1)^{l+m} {}_s S_l^m(\pi - \theta, a\omega), \quad (\text{A7})$$

$${}_s S_l^m(\theta; -a\omega) = (-1)^{l+s} {}_s S_l^m(\pi - \theta, a\omega), \quad (\text{A8})$$

and among the eigenvalues

$$-{}_s E_l^m(a\omega) = {}_s E_l^m(a\omega), \quad (\text{A9})$$

$${}_s E_l^m(-a\omega) = {}_s E_l^m(a\omega). \quad (\text{A10})$$

The constants ${}_s N_l^m$ are defined by the limiting behavior of the angular functions

$${}_s N_l^m \sim_{\theta \rightarrow 0} \theta^{l+m+sl} {}_s N_{l;0}^m(a\omega) \quad (\text{A11})$$

and

$${}_s N_l^m \sim_{\theta \rightarrow \pi} (\pi - \theta)^{l-m-sl} {}_s N_{l;\pi}^m(a\omega). \quad (\text{A12})$$

Owing to (A3) the constants for $s=+2$ are related to those for $s=-2$ by

$$384 {}_2 N_{l;0}^2 = (\text{Re}C) {}_{-2} N_{l;0}^2$$

and (A7) and (A8) provide

$$-{}_s N_{l;0}^m = (-1)^{l+m} {}_s N_{l;\pi}^m,$$

$${}_s N_{l;0}^m(a\omega) = (-1)^{l+s} {}_s N_{l;\pi}^m(-a\omega).$$

Our normalization has $(-1)^l {}_2 N_{l;\pi}^2(a\omega=0) > 0$.²⁸

In Sec. III we wrote down the short-range potential equation for the Kerr perturbations [Eq. (3.17)], due to Chandrasekhar and Detweiler.¹⁰

The variable Z in that equation is related to the Teukolsky functions by

$$K_{+2} Z = \frac{\rho^8}{\Delta^2} [Q - i\omega(W - 2i\omega f)] Y - \frac{\rho^8}{\Delta^2} (W - 2i\omega f) \frac{d}{dr_*} Y, \quad (\text{A13})$$

where $Y = (\Delta^2/\rho^3) {}_{+2} R$ and

$$\rho = r^2 + a^2$$

$$\alpha^2 = a^2 - \frac{am}{\omega},$$

$$Q = \frac{\Delta^2}{\rho^8} (F + \beta_2),$$

$$W = \frac{1}{F - \beta_2} \left(\frac{dF}{dr_*} - \kappa_2 \right) - 2i\omega(1-f),$$

$$f = 1 + \beta_2 \frac{\Delta^2}{\rho^8 V}, \quad (\text{A14})$$

$$K = \frac{\rho^8}{\Delta^2} Q f V - \frac{\rho^8}{\Delta^2} \left[W V + \frac{d}{dr_*} (fV) \right] \quad (\text{a constant}),$$

$$(W - 2i\omega f),$$

$$\Delta F = \nu \rho^4 + 3\rho^2(r^2 - a^2) - 3r^2 \Delta \equiv q,$$

$$\beta_2 = \pm 3\alpha^2,$$

$$\kappa_2 = \pm [36M^2 - 2\nu[\alpha^2(5\nu + 6) - 12a^2] + 2\beta_2\nu(\nu + 2)]^{1/2},$$

$$\nu = \lambda + 2s,$$

and r_* is defined up to a constant by

$$\frac{dr}{dr_*} = \frac{\Delta}{\rho^2}.$$

Then the potential V , called V_Z in Eq. (3.17), is given by

$$V_z = \frac{\Delta}{\rho^8} \left[q - \frac{\rho^2}{(q - \beta_2 \Delta)^2} \times \{ (q - \beta_2 \Delta) [\rho^2 \Delta q'' - 2\rho^2 q - 2r(q' \Delta - \Delta' q)] + \rho^2 (\kappa_2 \rho^2 - q' + \beta_2 \Delta') (q' \Delta - \Delta' q) \} \right], \quad (\text{A15})$$

a prime here denoting d/dr . Notice that ρ , ν , etc., in these equations have meanings different from their usual Newman-Penrose definitions. Owing to the four possible choices of signs for the constants β_2 and κ_2 there are four possible potentials. Reference 10 shows that each of the potentials yields the same reflection and transmission coefficients so that for the purpose of cross-section computation they are interchangeable.

The detailed behavior of the potential V has been discussed at length by Chandrasekhar and Detweiler in a series of papers.^{19, 15, 21} The general features of importance to our problem are discussed in Sec. III.

*Present address.

¹R. A. Matzner and Y. Nutku, Proc. R. Soc. London **A336**, 285 (1974).

²K. Schwarzschild, Sitzungsberichte Preuss. Akad. Wiss., 424 (1916).

³R. Kerr, Phys. Rev. Lett. **11**, 237 (1963).

⁴R. A. Matzner and M. P. Ryan, Astrophys. J. Suppl. **36**, 451 (1978).

⁵John William Strutt baron Rayleigh, Proc. R. Soc. London **A86**, 207 (1912).

⁶H. Jeffreys, Proc. Lond. Math. Soc. (2) **23**, 428 (1923).

⁷G. Wentzel, Z. Phys. **38**, 518 (1926).

⁸H. A. Kramers, Z. Phys. **39**, 828 (1926).

⁹L. Brillouin, Comp. Rend. **183**, 24 (1926).

¹⁰S. Chandrasekhar and S. Detweiler, Proc. R. Soc. London **A350**, 165 (1976).

¹¹S. A. Teukolsky and W. H. Press, Astrophys. J. **193**, 443 (1974).

¹²E. Newman and R. Penrose, J. Math. Phys. **3**, 566 (1962).

¹³P. L. Chrzanowski, R. A. Matzner, V. Sandberg, and M. P. Ryan, Phys. Rev. D **14**, 317 (1976).

- ¹⁴R. H. Boyer and R. W. Lindquist, *J. Math. Phys.* **8**, 265 (1967).
- ¹⁵S. Chandrasekhar and S. Detweiler, *Proc. R. Soc. London* **A345**, 145 (1975).
- ¹⁶W. G. Unruh, *Phys. Rev. D* **10**, 3194 (1974).
W. H. Press and S. A. Teukolsky, *Astrophys. J.* **185**, 649 (1973).
- ¹⁸S. A. Teukolsky, *Astrophys. J.* **185**, 635 (1973).
- ¹⁹J. Mathews and R. L. Walker, *Mathematical Methods of Physics* (Benjamin, N. Menlo Park, California, 1970).
- ²⁰R. A. Matzner and M. P. Ryan, *Phys. Rev. D* **16**, 1636 (1977).
- ²¹S. Chandrasekhar and S. Detweiler, *Proc. R. Soc. London* **A352**, 325 (1977).
- ²²I. S. Gradshteyn and I. M. Ryzhik, in *Table of Integrals, Series and Products*, 4th ed. (Academic, New York, 1965).
- ²³R. A. Breuer, M. P. Ryan, Jr., and S. Waller, *Proc. R. Soc. London* **A358**, 71 (1977).
- ²⁴J. M. Bardeen, in *Black Holes*, Les Houches Summer School, 1972, edited by C. M. DeWitt and B. S. DeWitt (Gordon and Breach, New York, 1973).
- ²⁵K. W. Ford and J. A. Wheeler, *Ann. Phys. (N. Y.)* **7**, 259 (1959).
- ²⁶F. L. Yost, G. Breit, and J. A. Wheeler, *Phys. Rev.* **49**, 174 (1936).
- ²⁷L. D. Landau and E. M. Lifshitz, *Quantum Mechanics, Non-Relativistic Theory* (Pergamon, London, 1958).
- ²⁸J. N. Goldberg, A. J. Macfarlane, E. T. Newman, F. Rohrlich, and E. C. G. Sudarshan, *J. Math. Phys.* **8**, 2155 (1967).